Hydrodynamics and Mass Transport in Wall-Tube and Microjet Electrodes: An Experimental Evaluation of Current Theory

Neil V. Rees, Oleksiy V. Klymenko, Barry A. Coles, and Richard G. Compton*

Physical and Theoretical Chemistry Laboratory, Oxford University, South Parks Road, Oxford OX1 3QZ, U.K.

Received: July 18, 2003; In Final Form: October 6, 2003

The application of steady-state and fast-scan linear sweep voltammetry to a high-speed wall-tube electrode (HWTE) is reported in different solvents to investigate the response of the HWTE over a wide range of Reynolds' numbers (*Re*). Experiments are reported for the oxidation of *N*,*N*,*N*′,*N*′-tetramethyl-*p*-phenylenediamine (TMPD) in propylene carbonate (PC), water, butyronitrile (BN), acetonitrile (AN), and acetonitrile−water mixture solutions containing 0.10 M supporting electrolyte for a 24 μm radius platinum microdisk electrode housed within the HWTE using a range of average flow jet velocities from 0.03 to 19.8 m s^{-1} (corresponding to volume flow rates of 0.003−0.25 cm^3 s^{-1} and center-line jet velocities from 0.05 to 39.5 m s^{-1}). Fast scan linear sweep voltammetry is presented for the oxidation of TMPD in PC and of 9,10-diphenylanthracene (DPA) in AN. Theoretical results are derived using finite element methods for both one- and two-dimensional mass transport models. It is found that, for solvents with a kinematic viscosity above ca. 7.5×10^{-3} cm^2 s^{-1}, the hydrodynamic behavior for $Re < 2000$ is as expected with current responses in accordance with those predicted for a laminar, parabolic inlet flow profile. In low viscosity solvents, where $Re < 2000$, currents are lower than expected, indicating a departure from laminar flow in practical cells even at low *Re*. The HWTE is compared to the channel electrode in the light of the experimental results, theoretical limits of electron-transfer rate detectable, and conclusions drawn that the channel electrode is more reliable for kinetic measurements.

Introduction

There has been considerable interest in the field of submerged, impinging jets in the fields of engineering and chemistry. Impinging jets, whether in the form of a gas or a liquid, are widely used for heat and mass transfer applications within industry because of their effective transport capabilities. Specific applications include turbine-blade cooling, paper drying, and electronics packaging. The engineering literature to date has mainly focused on the heat-transfer properties of impinging jets, but there has been some work in the area of understanding the more general flow fields of submerged jets, dealing with among others, the velocity distribution,[1,2] the nozzle-exit region,[3] the effects of nozzle geometry,[4] confinement of the volume entered by the jet,[5−7] and effect of the depth of liquid penetrated by the jet.[8]

For electrochemists, the impinging jet has found use as a hydrodynamic electrode where the jet is comprised of an electrolyte that crosses the filled chamber (usually of the same electrolyte composition) to strike an electrode situated directly opposite the nozzle. The hydrodynamics of this arrangement under laminar conditions consists of two different flow regimes in the vicinity of the electrode, as shown schematically in Figure 1. First, there is a stagnant region directly below the jet, where the flow is axial, which extends a distance of approximately one to three nozzle diameters across the flat surface.[9,10] Outside of this stagnant region is the "wall-jet" region where the radial velocity begins to decay.[11] In the limiting case where the electrode is entirely within the stagnant region (i.e. the nozzle diameter is greater than that of the electrode), the electrode is uniformly accessible and termed a wall-tube electrode (WTE),[12] as in the work considered here.

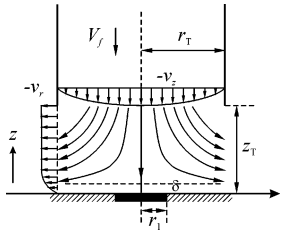

Figure 1. Streamlines and geometry of a WTE.

The WTE has been the subject of investigation in terms of its applications to mechanistic and analytical work,[13−16] and has been further developed by Unwin and co-workers utilizing microelectrodes to develop a microjet electrode.[17] This has been shown to be effective for investigating electron-transfer kinetics,[18] coupled solution reactions,[19] and flow analysis,[20] and a model has recently been developed to approximate the mass transport within it for Reynolds numbers of less than 2000.[21−23] The conclusions of this latter work were that the alignment of nozzle and electrode were critical to the currents measured. Not only was nozzle−electrode alignment key, but also the entire cell-construction required careful design as both the thickness of nozzle walls and nozzle−electrode separation were shown to play important roles in the formation and positioning of vortices within the cell. Finite element (FEM) simulations were used to demonstrate these effects, and also highlighted departures from the treatments for macrosized WTEs proposed by Albery and Bruckenstein[24] and Chin and Tsang[12] when considering the velocity behavior near the electrode. However, the

* To whom all correspondence should be addressed. E-mail: richard.compton@chemistry.ox.ac.uk. Telephone: +44 (0) 1865 275413. Fax: +44 (0) 1865 275410.

10.1021/jp030883r CCC: $25.00
Published on Web 11/15/2003

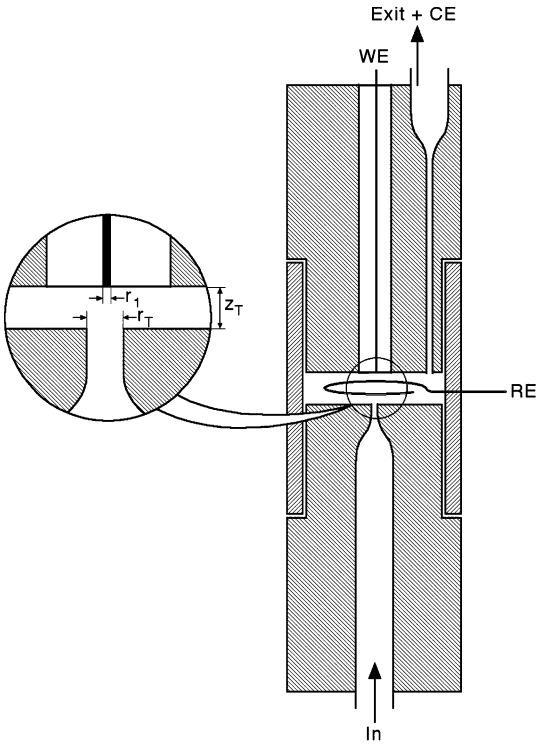

Figure 2. Schematic diagram showing the HWTE.

contribution to limiting current of radial diffusion was not found to be significant at an electrode of 50 μm diameter in flow rates above 8×10^{-4} cm^3 s^{-1}.[21] These radial diffusion effects were neither observed by Chin and Tsang nor considered by Albery and Bruckenstein, as their work was limited to macroelectrodes only.

In a recent paper we described a miniaturized WTE for use in a pressurized system[25] previously developed for channel electrode use.[26] This high-speed WTE ("HWTE", Figure 2) has been designed to operate at high volume flow rates achievable using the pressurized system, to measure fast electrochemical kinetics. The application of fast-scan linear sweep voltammetry was used to investigate the heterogeneous electron-transfer rate for the oxidation of *N*,*N*,*N*′,*N*′-tetramethyl-*p*-phenylenediamine (TMPD) in propylene carbonate (PC) at the HWTE and theory introduced to enable the simultaneous extraction of the values of k_0, α, and E_f^0, by fitting the complete voltammogram. This method was found to be in good agreement with independent high-speed channel electrode experiments.[25]

In this paper, we present results of steady-state and fast-scan voltammetry for the oxidation of *N*,*N*,*N*′,*N*′-tetramethyl-*p*-phenylenediamine (TMPD) and 9,10-diphenylanthracene (DPA) in a range of solvents in order to investigate the current−voltage response over a wide range of Reynolds numbers. With *Re* between 110 and 5700, the regions predicted to exhibit laminar ($Re < 2000$), transitional ($2000 < Re < 4000$), and turbulent ($Re > 4000$) hydrodynamic behavior are spanned.[12]

Theory

Wall-Tube Hydrodynamics: Ideal and Realistic Behavior. The first formulation of hydrodynamics in the WTE was attempted by Froessling[27] and considered a macroelectrode. This was based on a model of a jet issuing from a nozzle (radius r_T) at a given volume flow rate (V_f), travelling across the solution-filled chamber a distance z_T, before striking the electrode (radius r_1) placed normal to the direction of the jet, and flowing away radially in three dimensions. Several assumptions were then made to simplify the problem:

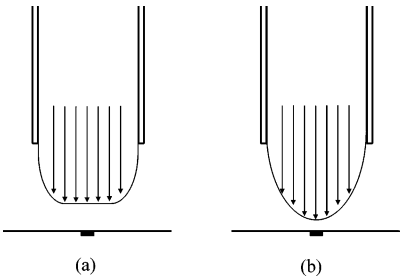

Figure 3. Schematic diagram illustrating (a) plug and (b) parabolic flow.

(i) There is a uniform velocity across the inlet, corresponding to plug flow immediately before and after the nozzle exit (thereby providing uniform accessibility as in Figure 3a).[21]

(ii) A constant radial velocity is imposed at a boundary extending from the side of the nozzle exit down to the hydrodynamic boundary layer (see Figure 1). The latter has a thickness δ.[21]

(iii) Radial diffusion is a negligible component of the total diffusive flux to the electrode.[23]

(iv) Any turbulence within the chamber (i.e., vortices[22]) would not affect mass transport to the electrode.

(v) The nozzle exit and the electrode are directly aligned.

(vi) The nozzle walls are semiinfinite in thickness.

The axial and radial components of solution velocity (u_z and u_r) in a viscous flow as in Figure 1, are[27]

$$u_z = -2f(z) \tag{1}$$

$$u_r = f'(z)r \tag{2}$$

where r and z are cylindrical coordinates with r the radial distance from the center of the electrode and z is the distance in the axial direction. $f(z)$ is a function defined by the equations of motion and continuity,[27] as formulated in the following equation:

$$\frac{\partial^3\Psi}{\partial\chi^3} + 2\Psi\left(\frac{\partial^2\Psi}{\partial\chi^2}\right) - \left(\frac{\partial\Psi}{\partial\chi}\right)^2 + 1 = 0 \tag{3}$$

Here Ψ and χ are given by

$$\Psi(\chi) = \frac{f(z)}{\sqrt{\alpha\nu}} \tag{4}$$

$$\chi = z\sqrt{\frac{\alpha}{\nu}} \tag{5}$$

Here α is a constant dependent on volume flow rate, and ν is the kinematic viscosity. Working from an initial power series expression for eq 3 derived by Homann,[27] Froessling obtained a numerical solution for the region close to the electrode with the following as the leading terms in the power series:[27]

$$u_z = -1.31\alpha^{3/2}\nu^{-1/2}z^2 \tag{6}$$

$$u_r = 1.31\alpha^{3/2}\nu^{-1/2}rz \tag{7}$$

These results were developed empirically from experimental data with macroelectrodes by Chin and Tsang,[12] who thus only considered normal diffusion, to derive an asymptotic solution to the mass transport equation. The resulting expression for the

mass transport coefficient, k_{MT}, is

$$k_{MT} = 0.85002D\left(\frac{\alpha}{\nu}\right)^{1/2} Sc^{1/3} g(Sc) \quad (8)$$

where D is the diffusion coefficient, and the Schmidt number, Sc, is given by

$$Sc = \frac{\nu}{D} \quad (9)$$

The function $g(Sc)$ is an asymptotic series in Sc, given by

$$g(Sc) = 1 - 0.084593Sc^{-1/3} - 0.0016368Sc^{-2/3} - 0.0057398Sc^{-1} + 0.0014288Sc^{-4/3} + \ldots \quad (10)$$

This function is independent of radial position, r, and tends to unity for large Sc. For a typical experiment, with, e.g., $\nu \approx 10^{-2}$ cm^2 s^{-1} and $D \approx 10^{-5}$ cm^2 s^{-1}, $Sc \approx 10^3$ and $g(Sc) \approx 0.9915187$.

For an ideal WTE, the limiting current would be given by

$$I_{lim} = nF\pi {r_1}^2 k_{MT}[A]_{bulk} \quad (11)$$

and by applying this to real WTEs, Chin and Tsang found a dependence on nozzle−electrode separation (z_T) as well as nozzle-exit flow. By using a least-squares fitting method applied to empirical data obtained for a range of nozzle geometries, the following relationship was found for laminar conditions and for $Re < 2000$ and $0.1 < r_1/2r_T < 0.5$:

$$k_{MT} \approx 1.51\left(\frac{D}{2r_T}\right) Re^{1/2} Sc^{1/2} g(Sc) \left(\frac{z_T}{2r_T}\right)^{-0.054} \quad (12)$$

where Reynolds number, Re, is as defined by[12]

$$Re = \frac{d\bar{U}}{\nu} \quad (13)$$

where d is the nozzle diameter, ν is the kinematic viscosity, and $\bar{U}$ is the mean solution velocity. Furthermore, they also investigated the case where $4000 < Re < 16000$, deemed the *fully turbulent* region, for the radius ratio $0.1 < r_1/2r_T < 1.0$. Again an empirical relationship was found in the form

$$k_{MT} \approx 1.12\left(\frac{D}{2r_T}\right) Re^{1/2} Sc^{1/2} g(Sc) \left(\frac{z_T}{2r_T}\right)^{-0.057} \quad (14)$$

Comparing (13) and (14), and observing the very weak power dependence in the last term, we note for diagnostic purposes that the ratio of limiting currents in laminar and fully turbluent regions is approximately $1.51/1.12 = 1.35$.

Albery and Bruckenstein[24] have also considered the WTE by analogy with the rotating disk electrode. They approximated the results of Chin and Tsang, and suggested that the final term in (12) contributed a maximum of 6% to the limiting current, in arriving at a further simplified form:

$$I_{lim} \approx 0.61nF\pi {r_1}^2 D^{2/3} \nu^{-1/6} \left(\frac{V_f}{{r_T}^3}\right)^{1/2} [A]_{bulk} \quad (15)$$

Both eqs 12 and 15 provide a good approximation for limiting currents measured within the HWTE, provided that the constraints on these simplified models are met in reality and that the cell geometry mirrors those forming the basis of the original Chin and Tsang empirical correlation. The applicability of these results is also dependent on the convective rates within the HWTE as the former are derived for the case of macroelectrodes, whereas the latter is of micrometer dimensions. Implicit in the work of both Albery and Bruckenstein, and Chin and Tsang, is the assumption that the inlet flow profile is laminar and parabolic (see Figure 3b). The WTE remains uniformly accessible under this assumption provided that the electrode is significantly smaller than the inlet nozzle in diameter, as illustrated.

In reality, there are five possible sources of departure from predictions of limiting current behavior based on the preceding models, which may become observable in practical WTE experiments.

(i) Inlet flow characteristics: the above models assume that the flow is laminar and not turbulent as the jet leaves the nozzle. The profile of the flow at that point is also assumed to be parabolic in cross section (vide supra).

(ii) Radial diffusion effects: if the flow rate is not sufficiently high with respect to the size of the microelectrode, radial diffusion will provide a noticeable and significant contribution to the limiting currents.[23]

(iii) Vortices: the formation of vortices within the cell chamber have been shown to be a direct consequence of the confinement of an impinging jet.[6,7,22] The position of these vortices depends on the cell geometry, nozzle−electrode separation, and flow conditions. The vortex typically moves away from the center of the cell as either flow rate or nozzle−electrode separation increase. The turbulent mixing within the chamber caused by these vortices may have a measurable effect on the voltammetric response, for example, it has been suggested that toroidal recirculation may enable entrainment of material into the jet.[7]

(iv) Nozzle wall thickness: this has been shown to have an effect on the limiting currents obtained where the cell flow-outlet does not extend around the whole circumference of the cell at the same height.[22] This effect is more pronounced if vortices are present in the cell.[22] It is necessary for the nozzle walls to be designed to have a thickness greater than 0.1625 cm in order for the limiting current to be independent of it.[22]

(υ) Nozzle−electrode positioning: the current−voltage response is highly sensitive to the relative positioning of the nozzle and electrode in the $x-y$ plane. Unwin and co-workers[18,23] have shown that as the electrode is moved radially from directly beneath the nozzle, the limiting currents first rise to a maximum value where $r = r_1$ before sharply falling away.

Simulation of Electron Transfer at a Wall-Tube Electrode. We consider a simple electron-transfer reaction in an axisymmetric WTE system (i.e., ignoring radial diffusion) using one-dimensional finite element methods. At the wall tube electrode surface (written as an oxidation)

$$A - e^- \underset{k_b}{\overset{k_f}{\rightleftharpoons}} B \quad (16)$$

where both A and B are kinetically stable on the time scale of the experiment, and the bulk solution contains only A before it enters the flow-cell. The forward and reverse rate constants are given by Butler−Volmer theory:

$$k_f = k_0 e^{[(1-\alpha)F]/[RT](E-E_f^0)}; \quad k_b = k_0 e^{-[\alpha F]/[RT](E-E_f^0)} \quad (17)$$

where k_0 (cm s^{-1}) is the standard electrochemical rate constant for heterogeneous electron transfer, E_f^0 is the formal potential of the A/B redox couple, α is the transfer coefficient, and R, T, and F have their usual significance.

The uniform accessibility property of the wall-tube electrode[12,24] allows us to solve the convective-diffusion equations only in the z direction[24] where the solution velocity is proportional to z^2:

$$v_z = -Cz^2 \tag{18}$$

The constant C is given by[24]

$$C = 0.52\left(\frac{V_f}{r_T^3}\right)^{3/2}\left(\frac{r_T}{z_T}\right)^{0.162}\nu^{-1/2} \tag{19}$$

where V_f is the volume flow rate ($cm^3\ s^{-1}$), ν is the kinematic viscosity ($cm^2\ s^{-1}$), r_T is the nozzle radius (cm), and z_T is the nozzle−electrode separation (cm).

The time-dependent convective-diffusion equation describing mass transport of species A to the electrode is

$$\frac{\partial a}{\partial t} = D\frac{\partial^2 a}{\partial z^2} + Cz^2\frac{\partial a}{\partial z} \tag{20}$$

where $a = [A]/[A]_{bulk}$.

The boundary condition at the electrode corresponding to Butler−Volmer kinetics is

$$D\left.\frac{\partial a}{\partial z}\right|_{z=0} = (k_f a - k_b b)_{z=0} \tag{21}$$

where k_f and k_b are given by eq 17 and the concentration tends to its bulk value with increasing distance from the electrode:

$$a|_{z\to\infty} = 1 \tag{22}$$

The mathematical model (eqs 20−22) was solved using the finite element technique in ref 28.

The simulation procedure developed in ref 28 for linear sweep voltammetry was used to generate theoretical current−voltage curves for subsequent comparison with the experimental ones.

To "extract" the values of k_0, α and E_f^0 from the experimental voltammograms we used the least-squares method which consists of minimization of the following functional:

$$MSAD(k_0,\alpha,E_f^0) = \frac{1}{M}\sum_{k=1}^{M}(I_{exp}(E_k) - I_{th}(k_0,\alpha,E_f^0,E_k))^2, \tag{23}$$

where $I_{exp}(E_k)$ is the experimental current corresponding to the potential E_k, $I_{th}(k_0,\alpha,E_f^0,E_k)$ is the theoretically predicted value of the current at E_k, and M is the number of experimental data points. The values of α, k_0 and E_f^0 were then found by minimization of MSAD (eq 23) using the modified Newton's method.[29] The main iterative formula of the modified Newton's method for minimization of a function f of a vector argument $\bar{x}$ is

$$\bar{x}^{(k+1)} = \bar{x}^{(k)} + \gamma_k[H^{(k)}]^{-1}\nabla f^{(k)} \tag{24}$$

where k is the iteration index, $H^{(k)}$ is the Hessian matrix (the matrix of second partial derivatives) of f evaluated at the point $\bar{x}^{(k)}$, $\nabla f^{(k)}$ is the gradient of f at the same point, and γ_k is an adjustable coefficient. All derivatives were calculated using finite-difference approximations.

Experimental Section

Reagents. Chemical reagents used were TMPD (Aldrich, 98%), 9,10-Diphenylanthracene (DPA, Aldrich, 99%) tetrabutylammonium perchlorate (TBAP, Fluka Puriss electrochemical grade, >99%), potassium chloride (Riedel de Haan, ≥ 99.5%), sodium perchlorate (Aldrich, 99%), PC (Fluka, purum, ≥ 99%), BN (Aldrich, 98%) and AN (Fisher Scientific, "dried distilled", >99.99%). These were of the highest grade available and were used without further purification. Ultrapure water was used for cleaning (UHQ grade) and had a resistivity of not less than 18 MΩ cm (Elga, High Wycombe, Bucks, U.K.). All solutions contained 0.10 M supporting electrolyte and were thoroughly degassed with argon (Pureshield argon, BOC Gases Ltd., U.K.). All experiments were conducted at a temperature of 294 ± 1 K, and viscosity data were used relating to the same temperature.

TABLE 1: Ranges of Reynolds Numbers for the Solvents Employed

solvent	$\nu/cm^2\ s^{-1}$ at 294 K	*Re*
PC	2.11×10^{-2}	$110 \le Re \le 550$
water	8.94×10^{-3}	$470 \le Re \le 1590$
AN/water (0.35 mole fraction water)	5.67×10^{-3}	$500 \le Re \le 2900$
BN	5.44×10^{-3}	$600 \le Re \le 3650$
AN	3.45×10^{-3}	$1500 \le Re \le 5700$

Instrumentation. The HWTE consists of a platinum microdisk electrode embedded in a miniaturized wall-tube cell connected within pressurized apparatus described previously.[29] Figure 2 shows a schematic representation of the electrode assembly. High volume flow rates are achieved by pressurizing the chamber containing the solution and electrode assembly up to 1.5 atm. The solution flows through the nozzle of the specially designed wall-tube cell and out to the exit which is at ambient atmospheric pressure. The range of volume flow rates available to the HWTE is determined by the choice of chamber pressure and also by the solution viscosity. For example in the case of propylene carbonate, volume flow rates of up to 0.12 $cm^3\ s^{-1}$ can be achieved (corresponding to average flow linear jet speeds of ca. 9.4 m s^{-1}, with center-line jet velocities of up to 18.9 m s^{-1}), whereas with acetonitrile the volume flow rate can reach 0.25 $cm^3\ s^{-1}$ (average flow linear jet speeds of up to 19.8 m s^{-1} and center-line jet velocities of up to 39.5 m s^{-1}).

In considering the solution flow, it is informative to consider the Reynolds number, and Table 1 gives the ranges of Reynolds number accessible using the HWTE for the solvents used in this work. This enables the regions of $Re < 2000$, where flow has been shown to be laminar,[12] and $Re > 2000$, where a transition to turbulent flow is predicted, to be investigated.

The "fast scan" potentiostat used was built in-house and has a scan rate of up to 3×10^4 V s^{-1} and was used with minimum filtering. This potentiostat is similar to that described and utilized by Amatore and co-workers[30−32] and is capable of achieving ohmic drop compensation by means of an internal positive feedback circuit. The potential was applied with a TTi TG1304 programmable function generator (Thurlby Thandar Instruments Ltd, Huntingdon, Cambs, U.K.) and the current recorded with a Tektronix TDS 3032 oscilloscope (300 MHz band-pass, 2.5 GS/s). Computer programs were written in Fortran77 and run on a Pentium IV 2 GHz PC, which was also used for data analysis.

Finite element simulations of the flow characteristics were carried out using a commercial finite elements fluid dynamics software package, FIDAP (version 8.52, Fluent Europe Ltd, Sheffield, U.K.), which has been used successfully for the WTE before.[21−23]

Wall-Tube Cell and Electrodes. The construction of the wall-tube cell and the in situ microdisk electrode have been described previously.[25] The relevant geometry is as follows:

nozzle diameter, $r_T = 127\ \mu$m, nozzle−electrode separation, $z_T = 300\ \mu$m, and the electrode radius (r_1), determined to be 24 μm according to reported methods.[33]

The working electrode was polished between experiments using alumina lapping compounds (BDH) of decreasing size from 3 down to 0.25 μm on glass and soft lapping pads (Kemet Ltd., U.K.). The polished electrode was cleaned with ultrapure water and then immersed in approximately 30% nitric acid and stored under ultrapure water between each use. The electrode was regularly checked under an optical microscope to ensure that it was not becoming recessed.

The counterelectrode was a smooth, bright platinum wire coil, and a silver wire (99.95%, Johnson Matthey plc, London, U.K.) was used as a pseudo-reference electrode.

General Experimental Method for Steady-State Measurements. The same procedure was adopted in all experiments using the HWTE to obtain steady-state voltammograms of the oxidations of TMPD and DPA.

A solution containing the electroactive material and 0.1 M supporting electrolyte in the solvent of interest was introduced into the pressure chamber of the apparatus and an initial pressure set. A linear sweep voltammogram was then recorded at a scan rate of 0.4 V s^{-1}, which yielded a steady-state response[34] enabling a limiting current to be measured. This was repeated at a range of chamber pressures to obtain a range of volume flow rates. A plot of the measured limiting currents against $V_f^{1/2}$ would usually be made, according to the equation for wall-tube cells, assuming laminar, parabolic inlet flow:[12,24]

$$I_{lim} = 0.6244nF\pi[A]_{bulk}D^{2/3}r_1^{\ 2}\nu^{-1/6}\left(\frac{V_f}{r_T^{\ 3}}\right)^{1/2}\left(\frac{r_T}{z}\right)^{0.054} \qquad (25)$$

where n, F, D, and $[A]_{bulk}$ have their usual meaning, V_f is the volume flow rate, ν is the solvent kinematic viscosity, and the other terms represent the geometry of the cell and electrode as shown in Figure 2. This equation is essentially a combination of eqs 11 and 12. The ease of use of eq 25 has supplanted the use of eq 15, which contains an error of up to 6% of limiting current due to the approximated final term.

Theoretical Results

Finite Element Simulations of the Flow Characteristics. The flow characteristics were modeled using the FIDAP software package (www.fluent.com), to calculate limiting currents for comparison with experimental data and with the one-dimensional theoretical model described above.

Simulation of the limiting currents was carried out in two steps. First, the flow was calculated using a full model (with the solver set to laminar) which included the entry tube and the tapering jet, and then the velocities found were transferred to a smaller model for the convection/diffusion and surface reaction calculation. Separation of the flow and the convection/diffusion simulations is practicable since the changes in concentrations of the chemical species do not significantly affect the solution properties. Simulations were performed on an IBM-compatible PC, with a Pentium 4 1.8 GHz processor and 1 Gb of memory; flow simulations typically required about 20 min, and the convection/diffusion simulations about 30 s.

The flow model was 30 mm long, comprising 19.4 mm of inlet tube of 5.3 mm diameter, followed by 10.3 mm of the tapering glass jet, and then the electrode chamber which was 300 μm (axial) by 1200 μm in diameter. As an axisymmetric problem, the mesh was defined on a radial plane extending from the axis to the periphery. A graded mesh of 11611 elements

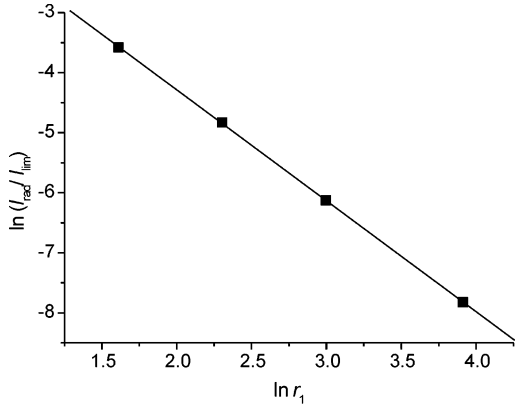

Figure 4. Plot of ln I_{rad}/I_{lim} vs ln (r_1/μm) for a typical aqueous system in the HWTE.

was used, with the finest mesh at the stagnation point, the smallest element being 0.028 μm (axial) by 0.49 μm (radial). The flow was specified as a parabolic axial velocity distribution at the inlet plane of the 5.3 mm diameter tube. The simulation used the segregated solver, which was run for 320 iterations, and achieved convergence of the FIDAP solution norm typically of 1.0×10^{-6}. To determine the flow profile in the jet, the axial velocities on a radial line 5.5 μm before the exit plane were read and fitted to an r^x curve using the Microsoft Excel spreadsheet solver. Deviations from the best fit r^x curve were small, typically 1−1.4%, so the use of a more complex function was not justified.

For the convection/diffusion calculation a smaller model sufficient to enclose the electrode and the diffusion layer was used, being a cylinder with axial length 5 μm and diameter 70 μm. Again, as an axisymmetric model, the mesh was defined on a radial plane and comprised 3740 elements. These were graded with smaller elements close to the electrode, having an axial dimension of 0.025 μm, which ensured typically 10 elements across the diffusion layer; the radial dimension was 1.27 μm close to the axis, but reducing to 0.13 μm at the edge of the electrode. The flow velocities found using the full model were transferred to the corresponding points on the small model using the Fidap FI-CONV function. The boundary conditions applied were bulk concentration c_0 at the upper face of the model, and the electrode was defined as a surface reaction entity with a fast forward reaction having $k_f = 1.0 \times 10^4$ cm s^{-1}. Simulation then solved for chemical species concentration only, using the segregated solver with the stiff chemistry option, which converged to a solution norm of 1.0×10^{-5} in 15 iterations. The value of the limiting current was then obtained using the FIPOST module to calculate the flux of material to the electrode.

FIDAP was also used to compute limiting currents using one-dimensional and two-dimensional models to observe the influence of radial diffusion for a typical aqueous system above ($D = 10^{-5}$ cm^2 s^{-1}, $\nu = 8.94 \times 10^{-2}$ cm^2 s^{-1}, $V_f = 0.03$ cm^3 s^{-1}). Figure 4 shows a logarithmic plot of the contribution to the total current by radial diffusion

$$\frac{I_{rad}}{I_{lim}}$$

(where $I_{lim} = I_{ax} + I_{rad}$) vs the electrode radius, r_1 (in μm). It was found that when $r_1 = 5\ \mu$m, radial diffusion contributes 0.8% to total current, rising to 2.8% for $r_1 = 2.5\ \mu$m. The main drawback of using such small electrodes within the WTE is the issue of cell construction and precise electrode alignment with the nozzle. These results show that it is acceptable to ignore

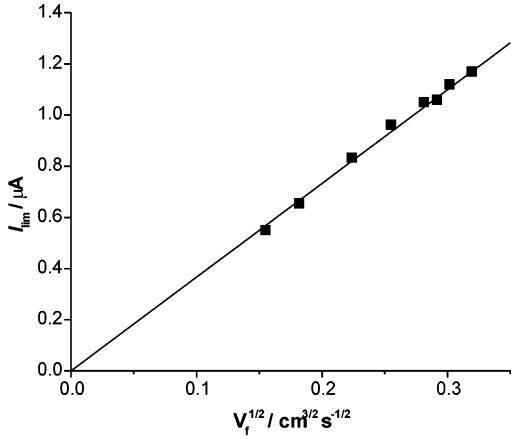

Figure 5. Plot of I_{lim} vs $V_f^{1/2}$ for 5.3 mM TMPD/0.10 M TBAP in PC ($R^2 = 0.988$).

TABLE 2: Variation in Flow Profile, r^x, with Solvent per FIDAP Calculations

solvent	V_f/cm^3 s^{-1}	r^x
PC	$0.003 \le V_f \le 0.12$	$2.0 \le x \le 2.7$
water	$0.04 \le V_f \le 0.15$	$2.7 \le x \le 4.2$
AN/water (0.35 mole fraction water)	$0.03 \le V_f \le 0.17$	$2.6 \le x \le 4.9$
BN	$0.03 \le V_f \le 0.19$	$2.7 \le x \le 5.0$
AN	$0.06 \le V_f \le 0.22$	$3.1 \le x \le 5.7$

radial diffusion effects in the present case where $r_1 = 25$ μm, which is in agreement with the experimental findings of Unwin et al.[13,17−20]

Experimental Results

To investigate the response of the HWTE to different solvent viscosities, both steady-state and transient voltammetry were recorded for comparison to theoretical predictions. First, we consider the steady-state case, as the limiting currents are easily extracted from experimental voltammograms and provide a reliable measurement for analysis. We then turn to the application of fast scan linear sweep voltammetry to the HWTE in order to observe whether experiment agrees with theory.

1. Steady-State Voltammetry at the HWTE. *Propylene Carbonate.* We first consider the first oxidation of TMPD in PC. A solution containing 5.3 mM TMPD and 0.1 M TBAP in PC was subjected to the experimental procedure outlined above, using a range of volume flow rates from 0.025 to 0.12 cm^3 s^{-1}. Figure 5 shows a plot of measured limiting currents against $V_f^{1/2}$ according to eq 25. Interpretation of the gradient in the figure using eq 25 yields a value for the diffusion coefficient of 3.0×10^{-6} cm^2 s^{-1}, in excellent agreement with the reported value of 3.1×10^{-6} cm^2 s^{-1}.[25] We conclude that at these low Reynolds numbers the flow profile as the jet leaves the nozzle in PC is laminar as expected.[12] The FIDAP simulations indicate that the inlet flow is also approximately parabolic (see Table 2), albeit with a small degree of "flattening" in the *z*-axis.

Water. Second, we consider the oxidation of TMPD in water, using a solution containing 4.0 mM TMPD and 0.1 M KCl. The above methodology was used over a range of volume flow rates from 0.04 to 0.16 cm^3 s^{-1}. Figure 6 shows a plot of measured limiting currents against $V_f^{1/2}$ according to eq 25.

Again, the gradient of this plot can be used to extract the value of the diffusion coefficient, being 4.3×10^{-6} cm^2 s^{-1}, which compares reasonably well with the previously reported value for the diffusion coefficient of 4.9×10^{-6} cm^2 s^{-1}.[35] We again conclude that at these Reynolds numbers ($Re < 1600$) in water the inlet flow profile is laminar.

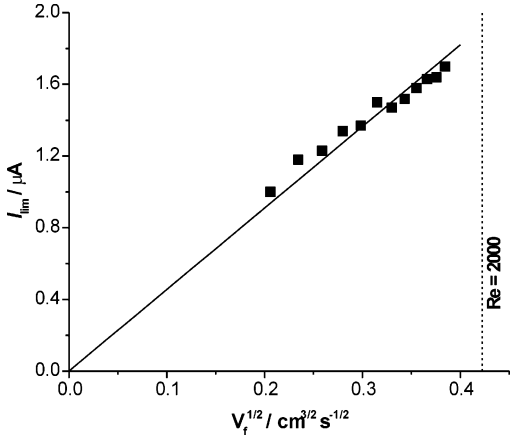

Figure 6. Plot of I_{lim} vs $V_f^{1/2}$ for 4.0 mM TMPD/0.10 M KCl in water ($R^2 = 0.916$).

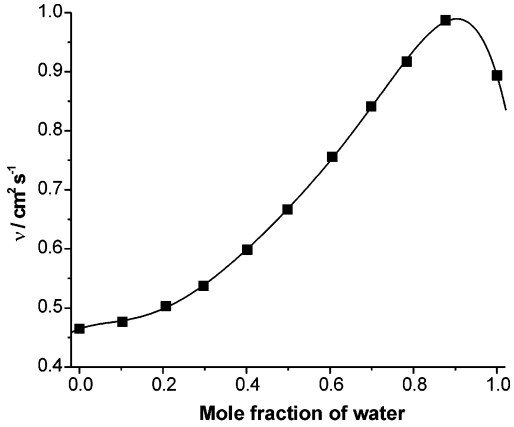

Figure 7. Plot of kinematic viscosity, ν vs molefraction of water, for AN/water mixtures, data from ref 31 ($R^2 = 0.999$).

Acetonitrile−Water Mixture. We next investigate the oxidation of TMPD in a binary mixture of acetonitrile and water within the HWTE under steady-state conditions. The exact mixture composition was 48.7 cm^3 of water and 51.0 cm^3 of acetonitrile, corresponding to a mole fraction of water of 0.35. This composition was selected based on an interpolation of published data[36] shown in Figure 7, having a kinematic viscosity of 5.67×10^{-3} cm^2 s^{-1} at the ambient temperature of the experiment (294K).

The diffusion coefficient of TMPD in this mixed solvent was obtained from cyclic voltammetry experiments conducted on a solution of 2.95 mM TMPD and 0.10 M sodium perchlorate in the binary mixture, measured at a glassy carbon disk electrode (diameter 3 mm). The peak currents extracted from the reversible voltammograms (peak separation ca. 60 mV) were plotted against square root of scan rate and gave a straight line as shown in Figure 8. Application of the Randles−Sevčik equation,[37]

$$I_p = (2.69 \times 10^5) n^{3/2} \pi r^2 D^{1/2} [A]_{bulk} \upsilon^{1/2} \qquad (26)$$

to the gradient of this plot yields a diffusion coefficient of $(8.4 \pm 0.5) \times 10^{-6}$ cm^2 s^{-1}. This compares with literature values of 4.9×10^{-6} [35] and 2.8×10^{-5} cm^2 s^{-1} [38] for the pure solvents of water and acetonitrile, respectively.

Next, a solution containing 2.95 mM TMPD and 0.1 M $NaClO_4$ in AN−water was introduced into the pressure chamber of the apparatus steady-state voltammograms measured as above, using a range of volume flow rates from 0.03 to 0.17 cm^3 s^{-1}.

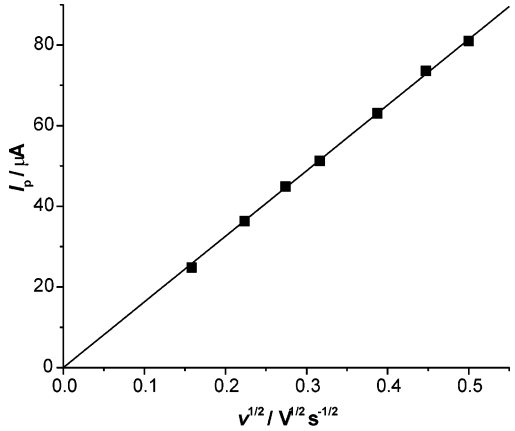

Figure 8. Plot of I_p vs $v^{1/2}$ for 2.95 mM TMPD/0.10 M $NaClO_4$ in AN/water mixure ($R^2 = 0.999$).

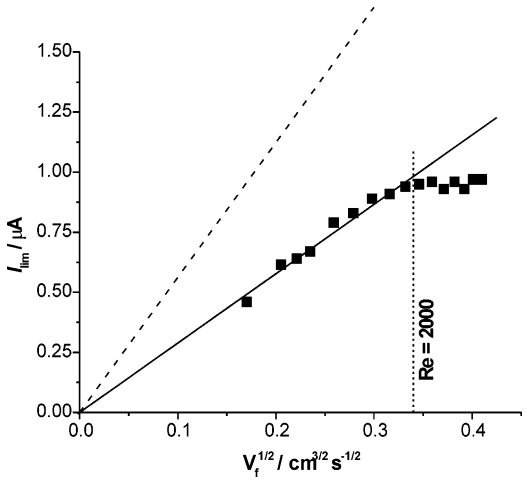

Figure 9. Plot of I_{lim} vs $V_f^{1/2}$ for 2.95 mM TMPD/0.10 M $NaClO_4$ in AN/water mixure. Dashed line indicates the theoretical response.

Figure 9 shows a plot of measured limiting currents against $V_f^{1/2}$, with a dashed line indicating the current response resulting from eq 25 using the above value for the diffusion coefficient. This plot displays two notable features.

First, there is a marked change in gradient of the plot at around $Re = 2000$ (marked as a vertical line on the graph). At lower flow rates, the current response is linear and passes through the origin. Beyond this transitional flow rate, however, the currents "level-off", and are almost independent of flow rate. This is as expected according to the observations of Chin and Tsang,[12] where the ratio between gradients in the laminar and *fully turbulent* regions is 1.51/1.12, indicating that the currents in the transitional region ($2000 < Re < 4000$, i.e., the present case for water) are relatively insensitve to flow rate. We believe the underlying reason for this effect is the turbulence within the jet acting to distribute the jet velocity across the jet front thereby reducing the center-line velocity at a fixed volume flow-rate. The effect of turbulence on velocity distribution within a jet has been elegantly shown by laser-doppler velocimetry by Fitzgerald, Morris, and Garimella.[6,7]

Second, the currents even in the $Re < 2000$ region are considerably lower than predicted by eq 25. This is discussed below.

Butyronitrile. The oxidation of TMPD in butyronitrile (BN) is next investigated. The kinematic viscosity for BN was found to be 5.44×10^{-3} cm^2 s^{-1} at 293 K from the literature.[39,40]

The diffusion coefficient of TMPD in this solvent was obtained from cyclic voltammetry experiments conducted on a solution of 4.87 mM TMPD and 0.10 M TBAP, measured at a glassy carbon disk electrode (diameter 3 mm). As before, the reversible voltammograms (peak separations ca. 60 mV) were analyzed to extract the peak currents, which were then plotted against the square root of scan rate according to eq 26. This gave a straight line as shown in Figure 10, and interpretation using eq 26 yields a diffusion coefficient of $(1.1 \pm 0.2) \times 10^{-5}$ cm^2 s^{-1}.

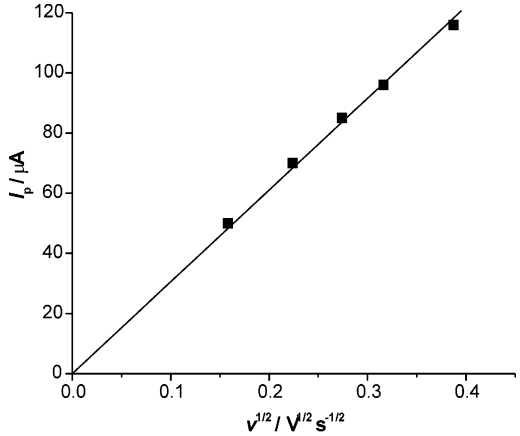

Figure 10. Plot of I_p vs $v^{1/2}$ for 4.87 mM TMPD/0.10 M TBAP in BN ($R^2 = 0.999$).

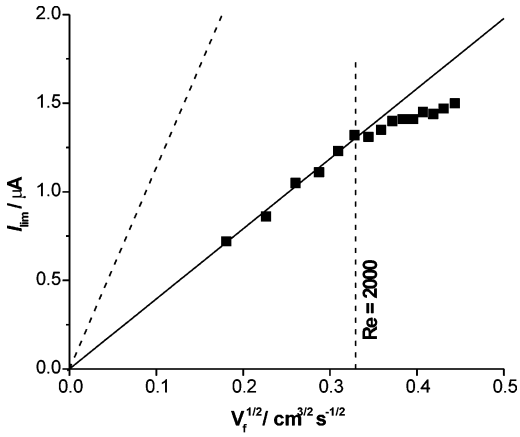

Figure 11. Plot of I_{lim} vs $V_f^{1/2}$ for 4.87 mM TMPD/0.10 M TBAP in BN ($R^2 = 0.989$). Dashed line indicates theoretical response.

Steady-state voltammograms were then recorded for this solution using the same methodology as before, over a range of volume flow rates from 0.03 to 0.20 cm^3 s^{-1}. Figure 11 shows a plot of measured limiting currents against $V_f^{1/2}$, with a dashed line indicating the current response resulting from eq 25 using the above value for the diffusion coefficient. As with the AN−water mixture, the range of data points straddles the $Re = 2000$ boundary and exhibits the same two features as for the mixture, namely the "dogleg" at ca. $Re = 2000$ and the lower-than-expected limiting currents in the region $Re < 2000$.

Acetonitrile. The steady-state voltammetry of the oxidation of a solution of 2.75 mM TMPD in 0.10 M TBAP in acetonitrile was recorded as above, using volume flow rates from 0.06 to 0.25 cm^3 s^{-1}. Figure 12a shows a plot of measured limiting currents against $V_f^{1/2}$, with a dashed line indicating the current response resulting from eq 25 using a previously reported value of 2.8×10^{-5} cm^2 s^{-1} for the diffusion coefficient.[38] As before, the limiting currents appear to be significantly lower than those expected on the basis of eq 25 for the region where $Re < 2000$.

Finally, a solution of 0.90 mM DPA in 0.10 M TBAP/AN was introduced into the pressure chamber and steady-state

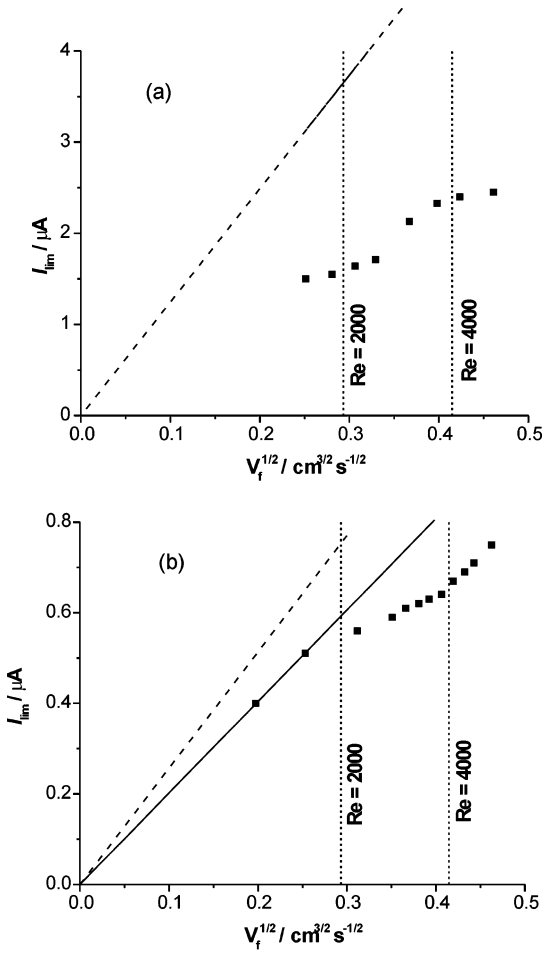

Figure 12. Plot of I_{lim} vs $V_f^{1/2}$: (a) 2.75 mM TMPD/0.10 M TBAP in AN; (b) 0.90 mM DPA/0.10 M TBAP in AN. Dashed line indicates the theoretical response in both plots.

voltammograms recorded over the same range of flow rates. Figure 12b shows a plot of measured limiting currents against $V_f^{1/2}$, with a dashed line indicating the current response resulting from eq 25 using a previously reported value of 1.4×10^{-5} cm^2 s^{-1} for the diffusion coefficient.[28] In this case, the figure shows two changes in gradient at approximately $Re = 2000$ and $Re = 4000$.

The ratio of the gradients in the $Re < 2000$ and $Re > 4000$ regions is 1.29, and this compares reasonably with the result derived by Chin and Tsang from aqueous experiments[12] where the expected ratio is given by $1.51/1.12 = 1.35$.

As before, the limiting currents appear to be significantly lower than those expected on the basis of eq 25 for the region where $Re < 2000$.

2. Fast Linear Sweep Voltammetry at the HWTE. *Oxidation of TMPD in Propylene Carbonate.* A solution of 2.86 mM TMPD and 0.10 M TBAP in PC was placed into the pressure chamber of the apparatus and the pressure set and capillary selected in order to achieve the required solution flow rate. A linear sweep voltammogram was then measured at this flow rate at a scan rate of 200 V s^{-1} and a transient response was obtained. Further linear sweep voltammograms were then recorded over a range of scan rates from 200 to 7000 V s^{-1} while the solution was flowing at volume flow rates ranging from 0.003 to 0.12 cm^3 s^{-1}.

Next, the voltammograms were amended by the subtraction of capacitative currents, which was achieved by subtracting the best-fit (least squares) line through the nonfaradaic signal, since the scan was of sufficient range to enable the nonfaradaic response to become established before the faradaic signal commenced. A combination of the use of a potentiostat capable of on-line correction for ohmic drop and the low current generated by a microelectrode within the HWTE makes adjustments for ohmic distortion unnecessary.[41] The current vs potential data for the voltammogram were then input into the computer program described above, and optimum values of k_0, α, and E_f^0 were obtained simultaneously by the least-squares method, using parameters set according to the experimental geometry and the flow rate used, as described in a previous paper by the authors.[25] The results were found to be $k_0 = (5.9 \pm 2.4) \times 10^{-2}$ cm s^{-1}, $\alpha = 0.46 \pm 0.08$, and $E_f^0 = 0.217 \pm 0.019$ V (vs Ag). The best-fit values of these parameters were then used to simulate a theoretical voltammogram and this compared to the experimental result. Figure 13 shows a selection of such plots, showing the excellent agreement observed in all cases.

Oxidation of DPA in Acetonitrile. A solution of 0.93 mM DPA and 0.10 M TBAP in AN was then placed into the pressure chamber, and linear sweep voltammograms were recorded over a range of scan rates from 100 to 8000 V s^{-1} while the solution was flowing at volume flow rates ranging from 0.03 to 0.25 cm^3 s^{-1}.

As before, the voltammograms were amended for the subtraction of capacitative currents. The current vs potential data for the voltammogram were then input into the computer program described above, but the values of k_0, α, and E_f^0 obtained were of a very poor MSAD rating, indicating a severe mismatch between theoretical and experimental results. Previous work has determined the kinetic parameters for the oxidation of DPA in AN to be $k_0 = 0.94 \pm 0.16$ cm s^{-1} and $\alpha = 0.53 \pm 0.02$.[29] By simulating theoretical voltammograms using these values, using the geometrical parameters of the HWTE, it is possible to compare a "true" theoretical result to the experimental voltammogram. Figure 14 shows a selection of such plots, showing that, in all cases, the experimental data show a reduced current response than should be expected, mirroring the results obtained using steady-state voltammetry.

Discussion

According to the wall-tube literature,[12−20] the nozzle flow field of the WTE is of steady, laminar parabolic flow for $Re < 2000$. Above a Reynolds number of 2000, the flow becomes unstable, passing through a transitional phase until full turbulence is achieved at around $Re = 4000$.[12] Empirical work on this has been based on aqueous systems,[12−20] and the above results for propylene carbonate and water support these published findings.

However, the less viscous solvents, AN−water, BN, and AN, do not follow this picture. Transitions are observed in the gradients of the plots of eq 25 at approximately $Re = 2000$ and $Re = 4000$ as expected, but the measured currents are significantly less than those predicted by eq 25 at all values of *Re*.

The existence of a plug-flow profile in the nozzle as opposed to a fully developed parabolic flow goes partway to explaining the loss of current in these less viscous solvents. This is because the center-line velocity is greater for parabolic flow then plug flow for a given volume flow rate (as illustrated in Figure 5). However, it appears that some degree of additional energy loss from the jet is required to fully account for the reduction in limiting currents. Fitzgerald and Garimella[6] have demonstrated that, in turbulent liquid jets at high Reynolds numbers, the jet

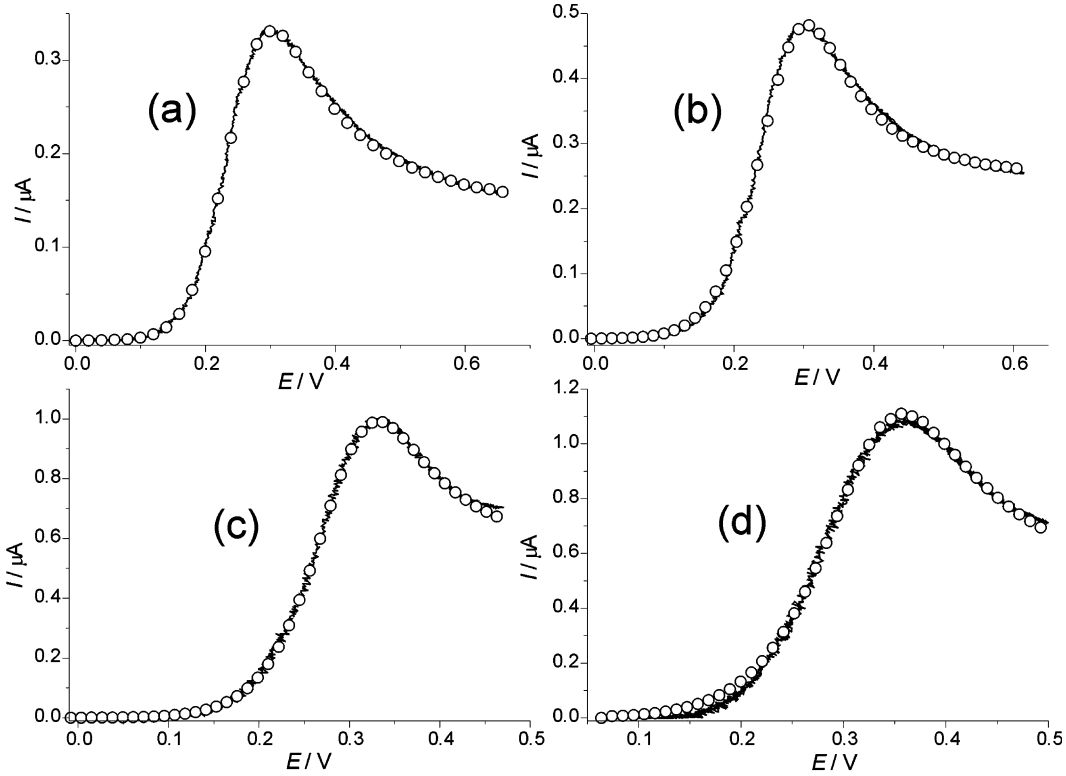

Figure 13. Comparison of experimental (—) and theoretical (○) current−voltage curves, based on the best-fit parameters obtained, for a selection of typical voltammograms recorded for a solution of 2.86 mM TMPD/0.10 M TBAP in PC: (a) $\upsilon = 240$ V s^{-1}, $V_f = 0.003$ cm^3 s^{-1}; (b) $\upsilon = 480$ V s^{-1}, $V_f = 0.012$ cm^3 s^{-1}; (c) $\upsilon = 1920$ V s^{-1}, $V_f = 0.065$ cm^3 s^{-1}; (d) $\upsilon = 2880$ V s^{-1}, $V_f = 0.030$ cm^3 s^{-1}.

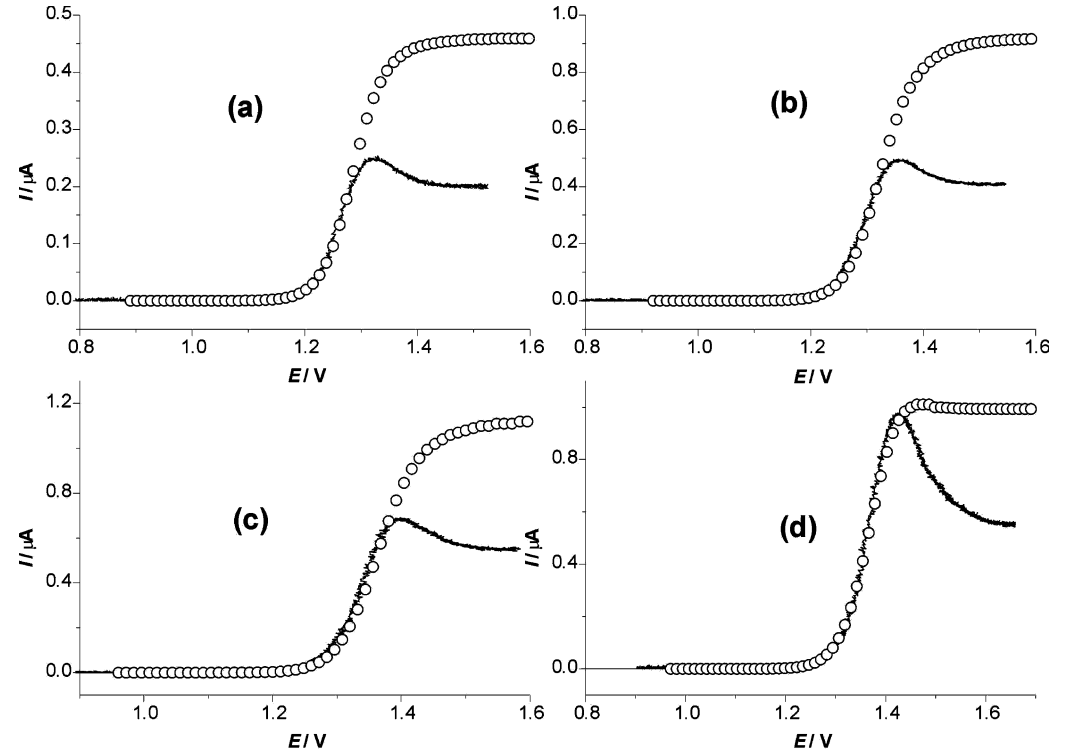

Figure 14. Comparison of experimental (—) and theoretical (○) current−voltage curves, based on the best-fit parameters obtained, for a selection of typical voltammograms recorded for a solution of 0.93 mM DPA/0.10 M TBAP in acetonitrile: (a) $\upsilon = 200$ V s^{-1}, $V_f = 0.03$ cm^3 s^{-1}; (b) $\upsilon = 800$ V s^{-1}, $V_f = 0.12$ cm^3 s^{-1}; (c) $\upsilon = 1600$ V s^{-1}, $V_f = 0.18$ cm^3 s^{-1}; (d) $\upsilon = 3000$ V s^{-1}, $V_f = 0.14$ cm^3 s^{-1}.

spreads out considerably between the nozzle exit and the opposite wall (i.e., electrode in this case), and turbulence/eddies at the edges of the nozzle exit rapidly spread inward toward the center of the jet, efficiently distributing the kinetic energy of the jet across the entire jet-front. Concurrently, the mean center-line velocity of the jet which gradually decreases as it travels across the nozzle−electrode gap, suddenly dies off when the jet-front reaches a distance of approximately 1.2 nozzle

diameters from the point of impact (the stagnation region) and can be as little as 75−85% of the initial mean jet velocity when it reaches the point of impact.[6]

Although these observations were recorded for fully turbulent liquid jets, it is possible that local roughness around the nozzle outlet, either on the inner walls or edge of the outlet, can produce a localized eddy, which could propagate across the jet in the less viscous solvents, averaging the distribution of flow velocities across the jet-front while spreading the jet radially.

In summary, the HWTE has been shown to be effective for viscous solvents such as PC or water. However, the electrode has severe limitations to its general usage.

First is the inlet flow characteristics. The assumption of laminar and either plug or parabolic inlet flow appears to break down in less viscous solvents. Second, the effects of radial diffusion become significant at electrode radii of the order of ca. 5 μm. Third, the flow field is very sensitive to the cell geometry of the WTE. The design and layout of the cell has been shown to have profound effects on the limiting currents measured.[21−23] This includes the thickness of the nozzle walls, the precise positioning of the electrode and nozzle, and the formation of vortices within the cell chamber.[21−23]

Comparison of Wall-Tube and Channel Electrodes. In light of these limitations on the universal applicability of high-speed wall-tube (and "microjet") electrodes, it is informative to compare the technique with another hydrodynamic method for measuring fast electrochemical kinetics, the channel electrode.

1. Limits of Measurement of Each Method. *Linear Sweep Voltammetry at the HWTE.* The range of k_0 which can be measured experimentally using linear sweep voltammetry in the HWTE has been investigated previously.[25] Using the curve-fitting procedure developed in that paper, and with experimental tolerance assumed to be 7.5%, voltammograms were simulated to obtain the minimum and maximum measurable values of k_0, having gradients 7.5% higher than the irreversible limit and 7.5% less than the reversible limit, respectively. The authors investigated the general current−voltage response to the normalized scan rate σ and the normalized heterogeneous rate constant K_{het},[28] given by

$$\sigma = 1.546\frac{Fv}{RT}D^{-1/3}\frac{r_T^3}{V_f}\left(\frac{z_T}{r_T}\right)^{0.108}\nu^{1/3} \qquad (27)$$

and

$$K_{het} = 1.602k_0D^{-2/3}\left(\frac{r_T^3}{V_f}\right)^{1/2}\left(\frac{z_T}{r_T}\right)^{0.054}\nu^{1/6} \qquad (28)$$

By considering the variation in voltammetry with respect to these normalized parameters, a general result can be obtained independent of the experimental geometry, solvent viscosity and flow rate. Figure 15 shows the result, with the empirical relationship for the lower curve given by the function

$$f(\sigma) = 0.1559\ln[1 + \exp\{3.151(\log_{10}\sigma - 0.3643)\}] - 0.7721 \qquad (29)$$

For all values of σ, it was found that the separation of the upper and lower curves was approximately 1.8, which lead to the following bounds for K_{het}:

$$f(\sigma) \le \log_{10}K_{het} \le f(\sigma) + 1.8 \qquad (30)$$

In practical terms, the ranges of measurable values of k_0 for

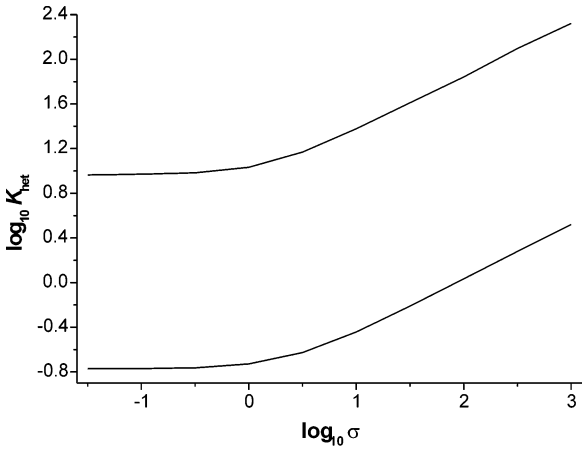

Figure 15. Upper and lower measurable limits of K_{het} as a function of σ in the HWTE.

different electrode radii (r_1), at steady state can be estimated using a typical flow rate but ignoring axial diffusion effects. For example, a typical aqueous system may have $D = 10^{-5}$ cm^2 s^{-1}, $\nu = 8.94 \times 10^{-2}$ cm^2 s^{-1}, and $V_f = 0.1$ cm^3 s^{-1}, and these limits would be

$$r_1 = 25\,\mu\text{m}, \quad 0.22 \le k_0/\text{cm s}^{-1} \le 1.41$$

$$r_1 = 12.5\,\mu\text{m}, \quad 0.61 \le k_0/\text{cm s}^{-1} \le 3.83$$

$$r_1 = 5\,\mu\text{m}, \; 2.29 \le k_0/\text{cm s}^{-1} \le 14.42$$

Linear Sweep Voltammetry at the HSChE. To view the discrimination limits available to the HWTE in context, a comparison was made with another hydrodynamic electrode used for fast kinetic measurement: the high-speed channel electrode (HSChE). Analogous simulations were therefore performed to investigate the range of k_0 values that could be measured using the HSChE described elsewhere.[28,29] Using the same methodology as above for the HWTE, and ignoring the effects of axial diffusion at the channel electrode,[28] the general $I-E$ response was simulated for the normalized scan rate σ and the normalized heterogeneous rate constant K_{het}, given by

$$\sigma = Fv\left(\frac{4h^4d^2x_e^2}{9V_f^2D}\right)^{1/3} \qquad (31)$$

and

$$K_{het} = k_0\left(\frac{2h^2dx_e}{3V_fD^2}\right)^{1/3} \qquad (32)$$

where cell half-height, $h = 54\,\mu$m, cell width, $d = 0.2$ cm, and electrode length $x_e = 12.5\,\mu$m and F, v, D, and V_f have their ususal meaning. By considering the variation in voltammetry with respect to these normalized parameters, a general result can be obtained independent of the experimental geometry, solvent viscosity and flow rate. Figure 16 shows the result, with the empirical relationship for the lower curve given by the function

$$g(\sigma) = 0.1173\ln[1 + \exp\{3.4399(\log_{10}\sigma - 3.6890)\}] - 0.6804 \qquad (33)$$

For all values of σ, it was found that the separation of the upper and lower curves was approximately 1.9, which lead to the

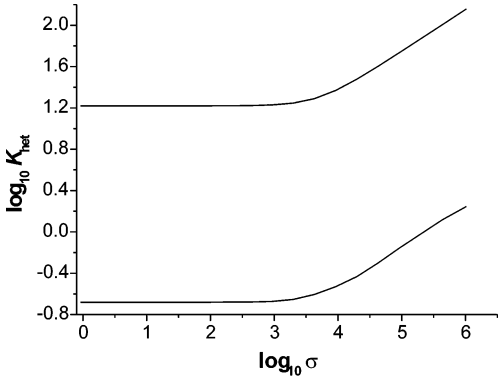

Figure 16. Upper and lower measurable limits of K_{het} as a function of σ in the HSChE.

following bounds for K_{het}:

$$g(\sigma) \leq \log_{10} K_{het} \leq g(\sigma) + 1.9 \qquad (34)$$

In practical terms, the ranges of measurable values of k_0 under *steady-state* conditions for different electrode lengths (x_e), at a typical flow rate, are

$$x_e = 40\ \mu\text{m}, \quad 10^{-3} \leq k_0/\text{cm s}^{-1} \leq 4.2$$

$$x_e = 12.5\ \mu\text{m}, \quad 10^{-2} \leq k_0/\text{cm s}^{-1} \leq 6.2$$

$$x_e = 5\ \mu\text{m}, \quad 10^{-2} \leq k_0/\text{cm s}^{-1} \leq 8.5$$

Previous work has shown that for the channel electrode, axial diffusion effects are negligible when the Peclet number, given by

$$P_s = \frac{3V_f x_e^2}{2dDh^2} \qquad (35)$$

is greater than 10^3.[28] For the typical volume flow rates involved, the effect of this restriction is that axial diffusion cannot be ignored for electrode lengths (x_e) of 2 μm or less.

Comparison of the HWTE and HSChE. The HWTE has a range of accessible k_0 values spanning approximately 1.8 orders of magnitude, and according to finite element simulations, it is capable of measuring heterogeneous electron-transfer rates approaching 15 cm s^{-1} without the effects of radial diffusion. However, its ability to measure fast kinetics, whether heterogeneous or homogeneous, is severely restricted by both the difficulties of constructing and aligning the nozzle with the electrode and the instability of its hydrodynamics. Earlier work on fast scan voltammetry in the HWTE has also shown that one-dimensional FEM methods can be used to accurately simulate the experimental $I-E$ response in propylene carbonate.[25] However, on moving to less viscous solvents, in which faster kinetic processes are expected to occur, the laminar and parabolic flow profile breaks down even at low Reynolds numbers ($Re < 2000$), leading to unknown hydrodynamics and reduced currents which cannot be simulated using existing theory.

Conversely, the HSChE, has been shown over several publications[26,29,42−46] to exhibit well-defined and reliable hydrodynamics at Reynolds' numbers approaching 9×10^3 [26,42] in a range of solvents. In all cases, the voltammetric data recorded have quantitatively agreed with theoretical results demonstrating the reliability of the HSChE for kinetic applications.

Conclusion

In light of the above results, it becomes apparent that in order to use the WTE for either kinetic or analytical purposes with any degree of confidence, it is necessary to confirm the nature of the hydrodynamics for the particular cell design and solvent system being investigated by ensuring that both steady-state and transient (cyclic) voltammetry agree with theory. In this way, the predictable hydrodynamic regimes of a particular WTE setup can be determined.

This has been illustrated in the above discussion where the HWTE has been shown to be effective for viscous solvents, yet cannot be used quantitatively in less-viscous solvents (e.g., acetonitrile).

Furthermore, unless independent measurements are made to verify the values of the parameters in eq 25, there is a risk that the approximate $I_{lim} \propto V_f^{1/2}$ relationship of limiting currents in the less viscous solvents may lead the experimentalist to believe the data are quantitative, when in fact the low current response may have simply been absorbed into variables within eq 25.

This emphasizes the importance of fast-scan voltammetry in verifying the flow characteristics, and so ensuring that only appropriate data are used for analysis. As shown by Figure 14, a comparison of such transient (linear sweep or cyclic) voltammograms with theory provides a definitive test of the current−voltage response, and we therefore recommend it as a diagnostic tool.

The range of kinetic parameters measurable by the HWTE has been shown to be comparable to that of the HSChE. The reproducibility of the flow conditions over all solvents thus far investigated in the latter electrode cell suggests that it is more reliable for the measurement of fast kinetics.

Acknowledgment. We appreciate the generosity of Professor C. Amatore and Dr. E. Maisonhaute in making available to us the designs for the fast-scan potentiostat apparatus developed in their laboratory. We thank EPSRC for a studentship for N.V.R. and the Clarendon Fund of Oxford University for partial funding for O.V.K.

References and Notes

(1) Andrade, E. N. C.; Tsien, L. C. *Proc. Phys. Soc. (London)* **1937**, *49*, 381.
(2) Coeuret, F. *Chem. Eng. Sci.* **1975**, *30*, 1257.
(3) Samuels, M. R.; Wetzel, D. M. *Chem. Eng. J.* **1972**, *4*, 41.
(4) Garimella, S. V.; Nenaydykh, B. *Int. J. Heat Mass Transfer* **1996**, *39*, 2915.
(5) Li, C.-Y.; Garimella, S. V. *Int. J. Heat Mass Transfer* **2001**, *44*, 3471.
(6) Fitzgerald, J. A.; Garimella, S. V. *Int. J. Heat Mass Transfer* **1998**, *41*, 1025.
(7) Morris, G. K.; Garimella, S. V.; Fitzgerald, J. A. *Trans. ASME, J. Electron. Packaging* **1999**, *121*, 255.
(8) Kuang, J.; Hsu, C.-H.; Qiu, H. *J. Eng. Mech.* **2001**, *127*, 18.
(9) Tani, I.; Komatsu, T. In *Proceedings of the 11th International Congress of Applied Mechanics*; Gortler, H., Ed.; Springer-Verlag: Berlin, 1966.
(10) Strand, T. *AIAA Pap. No.* 64−424.
(11) Glauert, M. B. *J. Fluid Mech.* **1996**, *1*, 625.
(12) Chin, D.-T.; Tsang, C.-H. *J. Electrochem. Soc.* **1978**, *125*, 1461.
(13) Macpherson, J. V.; Simjee, N.; Unwin, P. R. *Electrochim. Acta* **2000**, *47*, 29.
(14) Trevani, L. N.; Calvo, E.; Corti, H. *J. Chem. Soc., Faraday Trans.* **1997**, *93*, 4319.
(15) Kapauan, A. F. *Anal. Chem.* **1988**, *60*, 2161.
(16) Fitch, A. *J. Electroanal. Chem.* **1992**, *332*, 289.
(17) Macpherson, J. V.; Marcar, S.; Unwin, P. R. *Anal. Chem.* **1994**, *66*, 2175.
(18) Macpherson, J. V.; Beeston, M. A.; Unwin, P. R. *J. Chem. Soc., Faraday Trans. 1* **1995**, *91*, 899.
(19) Martin, R. D.; Unwin, P. R. *J. Electroanal. Chem.* **1995**, *397*, 325.
(20) Macpherson, J. V.; Unwin, P. R. *Anal. Chem.* **1999**, *71*, 4642.

(21) Melville, J.; Simjee, N.; Unwin, P. R.; Coles, B. A.; Compton, R. G. *J. Phys. Chem. B* **2002**, *106*, 2690.
(22) Melville, J.; Simjee, N.; Unwin, P. R.; Coles, B. A.; Compton, R. G. *J. Phys. Chem. B* **2002**, *106*, 10424.
(23) Melville, J. L.; Coles, B. A.; Compton, R. G.; Simjee, N.; Macpherson, J. V.; Unwin, P. R. *J. Phys. Chem. B* **2003**, *107*, 379.
(24) Albery, W. J.; Bruckenstein, S. *J. Electroanal. Chem.* **1983**, *144*, 105.
(25) Rees, N. V.; Klymenko, O. V.; Coles, B. A.; Compton, R. G. *J. Electroanal. Chem.* **2003**, *557*, 99.
(26) Rees, N. V.; Dryfe, R. A. W.; Cooper, J. A.; Coles, B. A.; Compton, R. G.; Davies, S. G.; McCarthy, T. D. *J. Phys. Chem.* **1995**, *99*, 7096.
(27) Cited in: Schlichting, H. *Boundary Layer Theory*; McGraw-Hill: New York, 1960; pp 81−83.
(28) Klymenko, O. V.; Gavaghan, D. J.; Harriman, K. E.; Compton, R. G. *J. Electroanal. Chem.* **2002**, *531*, 25.
(29) Rees, N. V.; Klymenko, O. V.; Maisonhaute, E.; Coles, B. A.; Compton, R. G. *J. Electroanal. Chem.* **2003**, *542*, 23.
(30) Amatore, C.; Lefrou, C.; Pfluger, F. *J. Electroanal. Chem.* **1989**, *270*, 43.
(31) Amatore, C.; Maisonhaute, E.; Simmonneau, G. *Electrochem. Commun.* **2000**, *2*, 81.
(32) Amatore, C.; Maisonhaute, E.; Simmonneau, G. *J. Electroanal. Chem.* **2002**, *486*, 141.
(33) Brookes, B. A.; Lawrence, N. S.; Compton, R. G. *J. Phys. Chem. B* **2000**, *104*, 11258.
(34) Brett, C. M. A.; Brett, A. M. *Electrochemistry. Principles, Methods and Applications*; Oxford University Press: Oxford, U.K., 1993; p 115.
(35) Albery, W. J.; Compton, R. G. *J. Chem. Soc., Faraday Trans. 1* **1982**, *78*, 1561.
(36) Aminabhavi, T. M.; Gopalakrishna, B. *J. Chem. Eng. Data* **1995**, *40*, 856.
(37) Bard, A. J.; Faulkner, L. R. *Electrochemical Methods: Fundamentals and Applications*, 2nd ed.; John Wiley: New York, 2001, p 231.
(38) Fernandez, H.; Zon, M. A. *J. Electroanal. Chem.* **1992**, *332*, 237.
(39) Harju, T. O.; Korppi-Tommola, J. E. I.; Huizer, A. H.; Varma, C. A. G. O. *J. Phys. Chem.* **1996**, *100*, 3592.
(40) Oswal, S. L.; Patel, N. B. *J. Chem. Eng. Data* **1995**, *40*, 840.
(41) Bard, A. J.; Faulkner, L. R. *Electrochemical Methods: Fundamentals and Applications*, 2nd ed.; John Wiley: New York, 2001, p 234.
(42) Rees, N. V.; Alden, J. A.; Dryfe, R. A. W.; Coles, B. A.; Compton, R. G. *J. Phys. Chem.* **1995**, *99*, 14813.
(43) Coles, B. A.; Dryfe, R. A. W.; Rees, N. V.; Compton, R. G.; Davies, S. G.; McCarthy, T. D. *J. Electroanal. Chem.* **1996**, *411*, 121.
(44) Prieto, F.; Aixill, W. J.; Alden, J. A.; Coles, B. A.; Compton, R. G. *J. Phys. Chem. B* **1997**, *101*, 5540.
(45) Prieto, F.; Hill, E.; Coles, B. A.; Compton, R. G.; Atherton, J. H. *J. Solid-State Electrochem.* **1999**, *3*, 187.
(46) Rees, N. V.; Klymenko, O. V.; Coles, B. A.; Compton, R. G. *J. Electroanal. Chem.* **2002**, *534*, 151.